https://doi.org/10.53256/COSE_230106

Diagnostic DO Transport Model for Narrow, Tidally Dominated Estuary

J.L DiLorenzo[a*], H.S. Litwack[b], G. R. Marino[c], P-S. Huang[d] and T. O. Najarian[e]
a Senior Oceanographer, Najarian Associates, 1 Industrial Way West, Eatontown, New Jersey, USA
b Senior Environmental Scientist, Najarian Associates, 1 Industrial Way West, Eatontown, New Jersey, USA
c Senior Environmental Analyst, Najarian Associates, 1 Industrial Way West, Eatontown, New Jersey, USA
d Senior Modeler, Najarian Associates, 1 Industrial Way West, Eatontown, New Jersey, USA
e President, Najarian Associates, 1 Industrial Way West, Eatontown, New Jersey, USA

[*]*Corresponding author: Joseph L. DiLorenzo, PhD, Senior Oceanographer, dilorenzo@najarian.com*

ABSTRACT: In 2010, an in-situ field-monitoring program was conducted in the Hackensack River Estuary (HRE) -- a narrow, tidally dominated, urban estuary located in New Jersey, USA. This program included: (1) automated sampling of Dissolved Oxygen (DO) concentrations, tidal elevations, currents, and other environmental variables, collected at several fixed mooring sites; and (2) discrete grab samples of DO and nutrient concentrations collected during an intensive field survey. The resulting dataset revealed the well-mixed characteristics of the Hackensack River Estuary (HRE), and tidal fluctuations of DO that were comparable to long-term variations. As a prelude to more complex modeling, a simple diagnostic model is developed to simulate fate and transport processes that control short-term DO variability in the lower reaches of the HRE directly from the combined datasets. The outcomes provide insights into the dominant dynamic processes and the impact of tides on the DO regime within the estuary's lower reach during the monitoring period. Such processes include tidal pumping, which imports DO into the lower HRE and disperses oxygen-demanding substances near a major point source. The present approach illustrates how simple diagnostic models may be used, in some circumstances, to synthesize available monitoring data, reveal dominant estuarine transport processes, and provide preliminary information that may better constrain future prognostic numerical model applications.

KEYWORDS: estuaries, dissolved oxygen (DO), estuarine fate and transport processes, in-situ monitoring, diagnostic models, tidal variability, dispersion, water quality, hypoxia, DO dynamics

1 INTRODUCTION

1.1 *Background*

The concentration of Dissolved Oxygen (DO) serves as an important indicator of the overall health of estuarine ecosystems. Understanding the multifaceted determinants that impact DO levels is an essential precursor to formulating environmentally responsible engineering projects in the marine environment.

For many years, analytical tools for dissolved oxygen (DO) modeling have concentrated primarily on variability across daily, synoptic, seasonal, and annual timescales. This focus is in acknowledgment of the intricate interplay of biogeochemical processes operating within this broad spectrum of temporal dynamics. However, with the advent of continuously recording DO sensors, there are new opportunities to develop high-temporal-resolution databases and DO models (e.g., Lucas, 2010; Lovato et al., 2013). Moreover, there is an increasing awareness of the importance of short-term, water quality variability within estuarine environments (e.g., Lucas et al., 2006; Hubertz and Cahoon, 1999; Nezlin et al., 2009) – especially in certain mesotidal, eutrophic estuaries. This paper provides an example of how the collection of high-temporal-resolution monitoring data (Marr et al., 2014) may further resolve short-term DO variability, quantify associated fate and transport processes, and provide an opportunity to improve preliminary water quality modeling and monitoring practices.

State-of-the-art estuarine modeling practices couple three-dimensional hydrodynamic and water quality models to simulate DO variability (Ji 2017). Deterministic water quality model formulations typically include fate and transport equations for multiple (typically 20+) state variables, each having source/sink terms. The coupled, biogeochemical transformation or reaction equations for these terms include many user-prescribed rate constants and source/sink terms that are not always well-constrained (e.g., Ganju et al., 2016). Consequently, there is always a chance that some kinetic processes may be over/underestimated, and that physical parameters may be adjusted unnecessarily to rectify inaccuracies.

Occasionally, simplified diagnostic models are used to help evaluate estuarine fate and transport processes directly and independently from field-monitoring data. Such models may provide a transparent means for identifying predominant estuarine controls prior to the application of complex numerical models. Though they may be based on intensive monitoring data, such models are constrained by their lack of predictive capabilities and often overlook crucial interactions essential for management applications. Nevertheless, information gleaned from such preliminary modeling procedures may serve as a valuable foundation for the refinement of more sophisticated models.

For example, Shen et al. (2008) use a simple, one-dimensional diagnostic model to characterize DO dynamics, and episodes of hypoxia, in the North Branch of Onancock Creek -- a small, well mixed estuary located along the Chesapeake Bay on Virginia's eastern shore. During dry summer periods, this estuary exhibits strong, diurnal DO oscillations, interspersed by periods of suppressed DO levels after large rainfall events. Given the limited influence of local tidal currents, the modeled DO dynamics in this context are shown to be controlled by phytoplankton, macroalgae, surface reaeration, net DO transport and organic carbon respiration. In contrast, tidal controls are dominant in the lower reaches of the urbanized HRE (DiLorenzo et al., 2004) – the area of the present diagnostic model study.

1.2 *HRE Characteristics*

The Hackensack River Estuary (HRE) constitutes a slender inland extension of the New York Harbor complex. It extends approximately 35 km southward from its head of tide at the Oradell Dam to its mouth, where it converges with the Upper Newark Bay and the Passaic River (Fig. 1). The HRE has an average centerline depth of approximately 7.6 m, with typical and maximum widths of approximately 150 m and 600 m, respectively. Mean tidal ranges vary from 1.59 m (at the mouth) to approximately 1.83 m (at the head). Above the HRE, the upper (non-tidal) Hackensack River drains a 292.7-km^2 watershed area and culminates at a large impoundment known as the Oradell Reservoir. Due to large reservoir withdrawals, the long-term-average freshwater inflow to the HRE (10.9 m^{3}s^{-1}) is small relative to the mean tidal discharge at the mouth (approximately 1,200m^{3}s^{-1}; Najarian Associates, 1990). A substantial proportion of the freshwater inflow, averaging around 33%, is contributed by a single municipal discharger, the Bergen County Utility Authority's (BCUA's) wastewater treatment plant (situated at km 20).

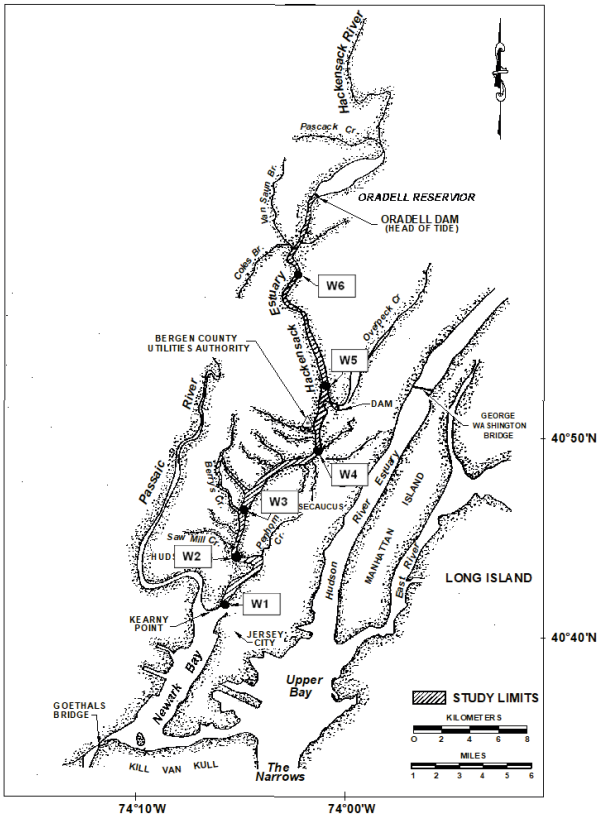

Figure 1: The HRE and adjacent tidal waterways

The average ratio of tidal to freshwater flow, approximately 110, is reflected in the system's low vertical salinity stratification (typically <1 psu), and low Estuarine Richardson Number (typically <0.001), as reported in previous studies (Najarian Associates, 1990, 2015). Due to its limited influx of fresh water and indirect connection with the open sea, the HRE undergoes a protracted flushing process and is intrinsically vulnerable to various sources of pollutants. These include wastewater dischargers, combined/storm sewers, local landfills, sediment deposits, upstream let-downs, atmospheric depositions and tidal exchange with Newark Bay. The HRE is further characterized by high nutrient levels and high algal productivity (e.g., Jung et al. 2021).

Phytoplankton assemblages in the upper HRE typically exhibit distinct characteristics throughout different seasons. During late autumn, winter, and spring, diatoms predominate, as observed in the study conducted by Foote (1983). Notable representatives within this diatom community include the resilient nanoplankton species Cyclotella menegheniana and Coscinodiscus rothii. In contrast, green algae assume dominance during dry summer conditions. However, blue-green algae persist

consistently and experience proliferation during prolonged wet-weather periods.

1.3 *Observed DO Variability*

The discernible impact of tidal forces on water quality within the Hackensack River Estuary (HRE) is evident through the analysis of field data collected in 2010 (ARCADIS, 2013). Tab. 1 provides an extensive outline of the comprehensive sampling strategy, which included continuous, long-term monitoring at several stations (Fig. 1) and a concentrated series of grab sampling activities carried out over a 5-day period.

Table 1: Overview of HRE field-sampling design during summer of 2010

Measured Variable*	Station Location	Sampling Frequency
tidal elev.	H1-H6	6 min.
ADCP cur. vel.	H1, H4	15 min.
DO, T, cond. pH.	W1-W5	15 min.
TSS, chl-a, CBOD5, NH3, NO3-, NO2-, TKN, TP, OP, TOC, DOC	W1-W5	3 hours
SOD, sed. TOC	W1, W3, W5	(monthly, 5 replicates)

*KEY: TSS = total suspended solids; CBOD5 = five-day carbonaceous biochemical oxygen demand; NH3 = ammonia; NO3- = nitrate; NO2- = nitrite; TKN = Total Kjeldahl nitrogen; TP = total phosphorus; TOC = total organic carbon; DOC = dissolved organic carbon; SOD = sediment oxygen demand.

Intensive data sampling included measurements of DO, Temperature, Turbidity, Conductivity, Salinity and pH,with readings taken every 15 minutes, at one-third and two-thirds depths, using YSI 6920V2-1 sondes. Additionally, tidal elevations were sampled every 6 minutes at up to six stations (W1 – W6 in Fig. 1) through the use of an Onset HOBO 30-foot depth titanium data logger (model U20-001-01-Ti). Tidal currents were sampled at 15-minute intervals at two stations (i.e., W1 and W4) using workhorse Sentinel Acoustic Doppler Current Profilers (ADCPs).

Fig. 2 displays a continuous dataset of DO measurements collected during June, 2010 at six distinct estuarine stations (referenced W1-W6). At lower-estuary stations W1 and W2, DO variations primarily exhibit semi-diurnal patterns and are synchronized with the tidal fluctuations Furthermore, the data reveal features associated with diurnal inequality, signifying unequal tidal ranges within a day, as well as fortnightly variability in the DO time series. In terms of vertical variability, the DO data reveal predominantly unstratified conditions.

At up-estuary stations W4, W5 and W6, DO variations exhibit considerable magnitude and erratic behavior. These fluctuations are primarily dominated by diurnal, semi-diurnal and longer-period influences. Moreover, at stations W5 and W6, short-term DO concentrations appear to be inversely associated with tidal activity, with peak concentrations occurring near low tide and with depressed, minimum DO concentrations occurring near high tide. Such inverse correlations between tidal height and DO concentration are indicative of potential influences from downstream point sources. These observations suggest that tidal advection of a mean longitudinal DO gradient may constitute a dominant process in the lower reaches of the HRE. To explore this issue, a simplified model was developed based on available monitoring data. The model was applied to the lower reaches of the HRE as a preliminary step before engaging in more detailed numerical model analyses.

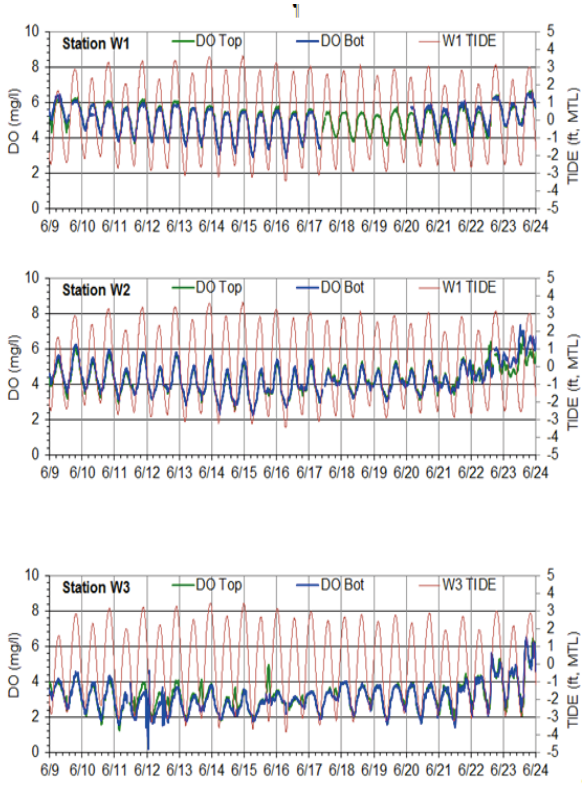

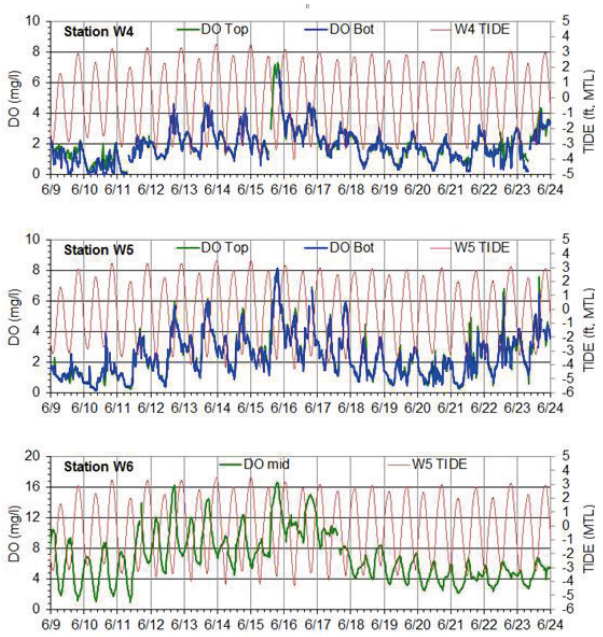

Figure 2: Time series plots of DO monitoring data at HRE stations W1 (upper panel) through station W6 (bottom panel) during June 2010. "DO Top" measurements applied at one-third depth; "DO Bot" at two-thirds depth.

2 MODEL DEVELOPMENT

2.1 *Model Formulation*

A simplified model is developed based on the continuous/intensive monitoring data and the narrow/shallow characteristics of the lower HRE. As noted above, vertical density stratification is relatively weak in this tidally dominated estuarine system (Fig. 3, top two panels). Likewise, vertical stratification of the sampled water quality variables is typically weak (Fig. 2 and Fig. 3). Thus, the formulation of a vertically integrated model is deemed appropriate for this case.

Lateral variability is not expected to be high in narrow reaches of well-mixed estuaries. Following Fischer et al. (1979 page 277), a representative time scale (t) for lateral mixing may be estimated from a representative width (W) and lateral dispersion coefficient (ε_t) of approximately 0.4 m^2/sec, a value applicable to a wide tidal river.

$$t \sim \frac{0.4W^2}{\varepsilon_t} = \frac{0.4*(150m)^2}{0.4^{m^2}/_s} = 6.3hrs \qquad (1)$$

This characteristic lateral mixing time is much shorter than estimated flushing times for the estuary, which are on the order of several tens of days. Therefore, lateral variations are also omitted from consideration in this preliminary model.

Accordingly, DO concentrations and other variables are assumed to exhibit uniformity in both the vertical and lateral dimensions. Consequently, the ensuing one-dimensional momentum and constituent transport equations are formulated below (Eqs. 2 and 3) as follows:

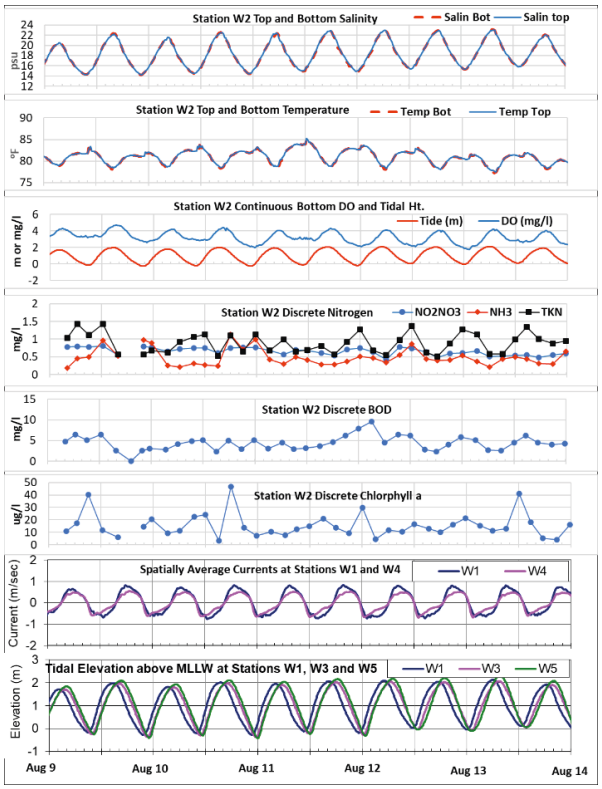

Figure 3: Representative continuous/discrete data collected at station W2 during the intensive field survey conducted during August 9-14, 2010.

$$\frac{\partial u}{\partial t} + u\frac{\partial u}{\partial x} + g\frac{\partial \eta}{\partial x} + \frac{gh}{2\rho}\frac{\partial \rho}{\partial x} + \frac{C_D u|u|}{h} = 0$$

(a), (b), (c), (d), (e) (2)

$$\frac{\partial [DO]}{\partial t} \approx -u\frac{\partial [DO]}{\partial x} + \frac{\partial}{\partial x}\left(K\frac{\partial [DO]}{\partial x}\right) -$$

$$k_C \frac{[CBOD5]}{1-e^{-5k_C}}\theta^{T-20} + 4.33k_N[TKN] +$$

$$k_s([DO]_s - [DO]) - SOD + 1.3 * 2.67 *$$

$$P_m \frac{I}{I_s} exp\left(1 - \frac{I}{I_s}\right)\theta_1{}^{T-20} B * \alpha - 2.67 * k_r * \alpha *$$

$$B * \theta_2{}^{T-20}$$

(a), (b), (c), (d), (e), (f), (g), (h), (i) (3)

KEY:
t = time;
x = along-axis distance (positive landward);
u = vertically averaged, along axis current velocity component (positive landward);
η = water surface elevation
ρ = water density
g = gravitational acceleration
h = average water depth
C_D = drag coefficient
[DO] = dissolved oxygen concentration;
[DO]s = dissolved oxygen saturation concentration
SOD = sediment oxygen demand
K = along-channel dispersion coefficient
I = irradiance
Is = saturation value of the irradiance
T = water temperature
k_C = CBOD decay coefficient
k_N = ammonia decay coefficient
k_s = reaeration rate coefficient formulated as: 7.6u $h^{-1.333}$ times $1.024^{(T-20)}$
P_m = maximum production rate
k_r = respiration constant
θ_2 = temperature adjustment factor (typically ~ 1.047)
B = algal biomass
[chl-a] = chlorophyll-a concentration
α = chlorophyll-a to carbon conversion factor

The simplified momentum balance equation (Eq. 2) encapsulates the influence of tidal processes within a shallow channel (LeBlond, 1978). Terms 'a' and 'b' represent the local and advective accelerations; terms 'c' and 'e' represent the surface slope and bottom friction terms, respectively. Despite assuming the domain to be predominantly well-mixed both vertically and laterally, an additional term 'd' (i.e., the baroclinic component of the pressure gradient) is included to account for minor contributions originating from density variations. Wind forcing is neglected here due to the limited fetch within the system.

The simplified fate and transport equation (Eq. 3) employed for this 5-day simulation bears similarity to the equation utilized by Shen et al. (2008), albeit with a significant addition pertaining to tidal advection. Term 'a' of Eq. 3 denotes the rate of change of dissolved oxygen concentration over time. Term 'b' represents the advective transport of dissolved oxygen along the channel, aligned with the principal axis. Term 'c' represents the corresponding dispersive transport. Collectively, terms 'd' and 'e' represent the ultimate biochemical oxygen demand (UBOD), encompassing both carbonaceous and nitrogenous components, with expressions formulated in terms of the measured concentrations of CBOD5 and TKN. Note that most of the CBOD5 measurements were found to be below the detection limit of 2 mg/l, introducing some uncertainty in term 'd.'. These non-detectable CBOD5 values were replaced by 0 in the model calculations. Term 'e' includes a slightly reduced stoichiometric factor (i.e., 4.33 vs. 64/14 or 4.57) to account for nitrogen demand (e.g., Ji 2007).

Term 'f' in Eq. 3 represents the re-aeration process. The coefficient governing re-aeration is contingent upon velocity, depth and water temperature, as detailed in the works of Ji (2007), Langbein and Durum (1967), and Churchill et al. (1962).

Term 'g' represents the measured sediment oxygen demand (SOD) (ARCADIS, 2013).

Term 'h' in Eq. 3 represents the oxygen production attributed to algae. This production is straightforwardly represented through the utilization of a maximum growth rate, P_M, the biomass parameter B, and growth-limiting functions associated with light (based on Steele), and temperature (Ji, 2007). It is assumed that growth is limited primarily by light intensity and temperature in this nutrient-rich and turbid estuary. The stochiometric factor of 1.3 is employed due to the assumption that nitrate serves as the primary source of dissolved oxygen (DO). Meanwhile, the stochiometric factor of 2.67 corresponds to the ratio of DO production relative to carbon production. This factor is integrated into the equation to account for the biomass input derived from measured chlorophyll-a concentrations (in units of ug/l) which are converted to carbon concentrations (in mg/l units) based on an assumed carbon-to-chlorophyll ratio.

Finally, term 'i' in Eq. 3 is indicative of respiration, which is likewise assumed to be proportional to Phytoplanton biomass, incorporating an Arrhenius-type temperature

dependency (e.g., Ji, 2007). Admittedly, alternate formulations could have been chosen for all of the modeled source/sink terms. Nevertheless, as shown below, the tidal signal within the lower estuary remains sufficiently prominent, rendering intricate formulations unnecessary at this stage. Moreover, the model's spreadsheet format facilitates user-friendly visualization of the potential effects of alternative formulations, which may either prove to be less sensitive or improve model accuracy.

The model parameter values chosen for this application were selected based on estimates available in the literature (e.g., Lung 1993).

Table 2: Representative model parameter values for the HRE

Model Parameter/Rate	Symbol	Assigned Value
drag coef.	C_D	0.025
avg. water depth	h	7.6 m
reaeration coef.	k_s	0.4/d
sed. oxy. demand	SOD	$9.5x10^{-7}$ mg/l/s
C to chl-a ratio	α	30
sat. value irradiance	I_s	7500 BTU/ft^2/d
CBOD decay coef.	k_c	0.1/d
NH3 decay coef.	k_N	0.1/d
temp. adj. factors	Θ1,Θ2, Θ3	1.047, 1.068, 1.08
max. prod. rate	P_m	1.8/d
respiration rate	k_r	0.2/d
disp. coef., sta. W2	K	280-436 m^2/s

2.2 *Data Smoothing/Finite Differencing*

The following procedure was used to evaluate the terms in Eq. 2 and Eq. 3. First, the robust sampling period spanning from August the 9th to August the 14th, 2010 was selected. This period coincided with the intensive field survey and the deployment of moored sensors. The continuous (i.e., 15-minute-interval) monitoring data and discrete (3-hour-interval) sampling data (ARCADIS, 2013) were assembled for this timeframe. Subsequently, these datasets were interpolated slightly to attain a standard 15-minute time step.

Next, finite-difference approximations were used to estimate the various terms in Eq. 2 and Eq. 3. To approximate the time derivatives, a center-differencing scheme was chosen. The selection was based on the advantage of having knowledge of the 'future' values of measured variables (e.g., DO, u, T, etc.) at each modeled time step (15-minute), which distinguishes this approach from predictive modeling methods:

$$\frac{\partial u}{\partial t} = \frac{u(t+\Delta t)-u(t-\Delta t)}{2\Delta t} + O(\Delta t^2) \qquad (4)$$

This approach employed a second-order accurate (central-differencing) scheme to estimate the 'observed' local time rates of change terms for u and DO in Eq. 2 and Eq. 3 (vs. 'computed' rates that sum the modeled processes). However, this introduces complexities owing to the amplification of 'noise' inherent in monitoring data, particularly in electronically monitored DO concentrations. Such noise becomes magnified when finite differences are computed (e.g., Chartrand, 2011). Thus, the analysis was performed both with and without application of a common smoothing filter (i.e., a Stavitzky-Golay (S-G) filter; Stavitzky and Golay, 1964). This filter facilitates a moving-polynomial fit to the slightly noisy data. In this case, the moving fit at each time point was based on a second-order polynomial and 7 data points (three on each side of the point, each separated by 15-minutes). The application of this filter extended to the monitored DO, tidal current and tidal elevation time series throughout the modeling period from August 9th to August 12th, 2010. Note that comparable results were also obtained using a simple, 1-hour moving-average filter. However, as suggested by Ahnert and Abel (2007), the use of a moving average filter resulted in a slight reduction of some extreme values.

Using the velocity and elevation data, the velocity gradient, surface slope and density gradient terms in Eq. 2 were approximated based on a forward-differencing scheme. This estimation involved the utilization of representative along-axis current velocities obtained from the closest monitoring stations. (i.e., station W4 speeds were used to calculate station W4 terms and station W1 speeds were used in station W2 calculations).

$$\frac{\partial u}{\partial x} = \frac{u(x+\Delta x)-u(x)}{\Delta x} + O(\Delta x) \quad (5)$$

The spatial gradient terms obtained through this process possess first-order accuracy. However, spatial gradients of tidal elevations and current within the HRE exhibit relatively small variations when compared to a full cycle of variation (Fig. 3, lower panels). Consequently, the use of the forward-difference scheme to provide a first-order estimate is considered appropriate in this case.

To this end, a three-point spline interpolation method was applied to interpolate the available elevation data observed at stations W1, W3 and W5 during each modeled time step. Subsequently, the elevation gradient (of the surface-slope term in Eq. 2) was computed by applying a forward-difference operator over a relatively short upstream distance (500m) starting from station W1 along the smoothed series.

Similarly, forward-differencing schemes were used to estimate the concentration gradients associated with the advective transport and turbulent diffusion (second-derivative) terms. DO concentrations vary moderately among lower HRE stations W1 and W2, but tend to fluctuate markedly at up-estuary stations (Fig. 2). Furthermore, the influence of tides is less conspicuous in the upper HRE. Thus, the subject differencing scheme was not applied in the upper HRE. Instead, the present analysis focuses on the lower HRE.

2.3 *Dispersion Coefficient Calculations*

The model necessitates input data pertaining to longitudinal DO dispersion coefficients. Such coefficients (and dispersive fluxes) may be estimated directly from the high-temporal-resolution measurements of salinity, DO and other variables.

The comprehensive, tidally-averaged flux across a given cross-sectional area is the summation of the mean advective flux (driven by river flow) and the dispersive flux originating from several mechanisms (Fisher et al., 1979; Lucas, 2010). Temporal and spatial variations in estuarine velocities and material concentrations over a tidal cycle contribute to those dispersion mechanisms (which include tidal dispersion). An estimate for the longitudinal dispersion coefficient may be derived by summing those dispersive fluxes.

As noted above, the HRE experiences very limited freshwater flow (averaging 10.9 m^3s^{-1}). Consequently, the mean advective flux in this estuary remains constrained . Nonetheless, the HRE is likely to exhibit significant tidal dispersion, primarily due to the topographic variations and shoreline irregularities (e.g., marsh coves) that occur within a tidal excursion (Geyer and Signell, 1992). It is worth reiterating that vertical stratification and lateral gradients in the HRE are weak. Associated shear dispersion mechanisms are assumed to be secondary processes and are not factored in this estimate. The contributions to the dispersive flux are assumed to be dominated by tidal dispersion.

To evaluate tidal dispersion coefficients, the instantaneous flow velocity within the channel, denoted by u, and constituent concentration, c, may be dissected into components representing a tidal mean and tidal fluctuation (Dyer, 1977):

$$c = \langle c \rangle + c' \quad (6)$$

$$u = \langle u \rangle + u' \quad (7)$$

Here, the notation '< >' denotes the tidal mean, while the primed quantities represent the instantaneous tidal fluctuations relative to the mean. The average tidal flux of a constituent through a cross-sectional area, σ, is expressed as follows:

$$\sigma\langle uc \rangle = \sigma\langle u \rangle\langle c \rangle + \sigma\langle u'c' \rangle \quad (8)$$

Considering that vertical and lateral variations are not considered in this context, , the final term in Eq. 8 represents the dispersive flux through a cross-sectional area attributed to ‘tidal pumping’ (Fischer et al., 1979):

$$\sigma\langle u'c' \rangle = \sigma\langle (u - < u >)(c - < c >) \rangle \quad (9)$$

The emergence of the tidal pumping flux and its contributions to tidal dispersion can be attributed to the fact that the tidal mean of the product of the current speed and concentration in Eq. 8 is

not equivalent to the product of their individual averages.

Mathematically, it follows that the tidal pumping flux is a consequence of semi-diurnal variations (flooding and ebbing) of u and c that are not exactly in quadrature (Dyer, 1997; Fram et al., 2007). From a physical standpoint, the tidal pumping mechanism has been associated with different horizontal flow patterns on either side of the mouth of a well-mixed estuary (i.e., jet-like vs. distributed flow), and variations in flood and ebb concentrations near the estuary mouth (Fischer et al., 1979). Additionally, it's important to note that the tidal pumping mechanism consistently operates in a down-gradient manner (Lucas, 2010). Thus, the tidal pumping flux of DO in the lower reaches of the HRE is directed up-estuary, since DO concentrations generally decrease landward (Fig. 2).

The longitudinal tidal dispersion coefficient, K, may be calculated from the tidal pumping term by assuming a simple (Fickian) gradient transport relation:

$$K\frac{\Delta c}{\Delta x} = \langle (u - < u >)(c - < c >) \rangle \qquad (10)$$

Application of Eq. 10 for observed salinities and current speeds recorded during each tidal cycle during from August 9th to August 14th, 2010 at lower HRE station W2 yields K values between 280 m^2/s and 436 m^2/s (averaging 358 m^2/s), which were incorporated into the diagnostic model's dispersive transport term.

Furthermore, the continuous DO data were used to compute dispersive fluxes of DO at Station W2. For an average cross-sectional area at station W2 of approximately 1,600 m^2, the average up-estuary tidal pumping flux of DO at Station W2 exhibited a range between approximately 0.09 kg/s (324 kg/hour) and 0.23 kg/s (828 kg/hour) during the study period. These dispersive fluxes partially ventilate the Lower HRE.

3 RESULTS

Fig. 4 displays an application of the model to the lower HRE at station 3.

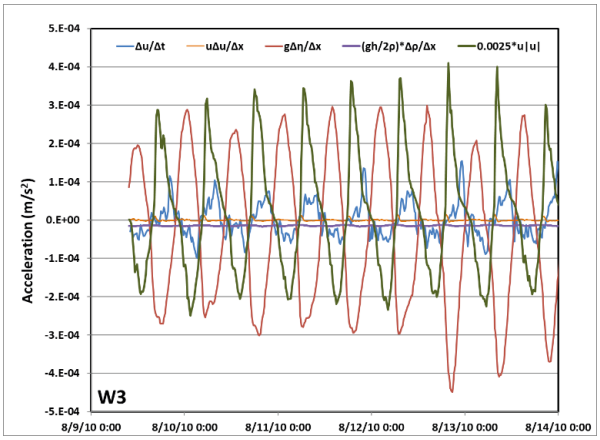

Figure 4: Computed dynamic force balance at station W3.

Though approximate, the model illustrates the prevailing dynamic force balance, which is primarily governed by surface slope and bottom friction terms. In contrast, the computed baroclinic forcing is relatively small due to weak density stratification. Likewise, advective inertia term exhibits a relatively modest magnitude. The local inertia term, on the other hand, remains relatively small during the peak-flood and ebb tide intervals, but gradually increases to peak values just before current reversals, occurring during slack-tide periods (i.e., when the friction term vanishes).

Likewise, application of Eq. 3 results in a time series (Fig. 5) that quantifies the relative contributions of individual fate and transport terms to DO variability at station W2. For example, the first (top) panel of Fig. 5 juxtaposes the calculated terms on the right-hand side of Eq. 3 (i.e., advective/dispersive transport, BOD decay, reaeration, SOD and P-R). Note that the computed terms for photosynthesis and respiration are combined here (as P-R) for ease of display.

The middle panel of Fig. 5 compares the sum of these terms (i.e., 'RHS') to the 'observed' time rate of change of DO (i.e., to the centered-differenced approximation on the left-hand side of Eq. 3). The bottom panel also compares the sum of these terms to the 'observed' time rate of change of DO, but with the latter smoothed by applying the 7-point S-G filter to the DO gage data.

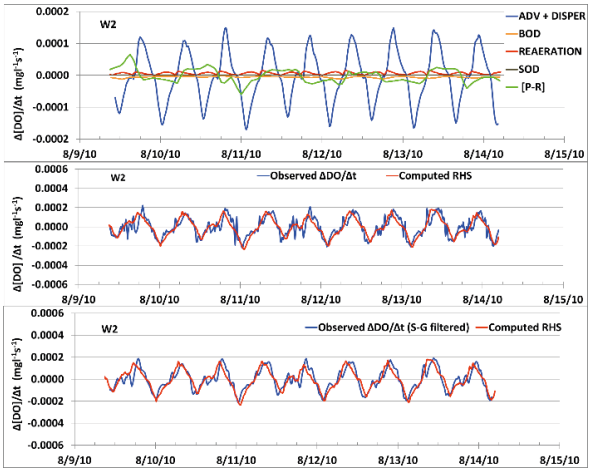

Figure 5: Computed DO dynamic balance at station W2 during intensive field survey. Upper panel: comparison of calculated fate and transport processes (on right side of Eq. 3). Middle panel: comparison of calculated time rate of change of observed oxygen concentration with the summation of simulated fate and transport processes (in upper panel). Bottom panel: same as the middle panel, but with 1-hour running average applied to the raw DO measurement data.

As noted above, smoothing was employed here to mitigate noise magnification that tends to arise when numerical differencing schemes are applied to field data exhibiting minor fluctuations. Fig. 6 illustrates the corresponding results at station W4.

As illustrated, the simplified model integrates the available datasets and displays the relative contributions of various control factors on short-term DO variability. This ability to synthesize the available monitoring data, and assess dynamic balances transparently constitutes a fundamental advantage of the adopted approach. The simulated advective transport provides the greatest contribution to DO variability at lower HRE station W2 ('transport' in Fig. 5, top panel). UBOD serves as a DO sink here. The computed re-aeration term exhibits relative modesty and varies with the semi-diurnal current speed. SOD also is relatively small. While significant, the computed P-R term does not dominate the DO dynamics at this specific location and during this particular season. Nonetheless, it appears to be a more dominant source of diurnal DO variability in the middle and upper HRE. Overall, the calculations suggest that tidal advection largely governs DO dynamics at lower HRE station W2 over the simulation period. Moreover, results indicate that the basic dynamic balance delineated by Eq. 3 accounts for the predominant diurnal and semi-diurnal variability at W2 (Fig. 5, middle and bottom panels). However, very short-term variability (< 3 hours) is not reproduced by the model.

In the upper HRE at station W4 (River Kilometer 17.4), the relative contribution of photosynthesis and respiration increases (Fig. 6, upper panel), and the model accuracy decreases (lower panel). Notably, contributions from the P-R term appear to vary inversely with irradiance, with heightened simulated production occurring on days with low cloud cover. Concurrently, BOD decay consistently exerts a secondary, yet substantial, DO sink. Conversely, the contributions of reaeration and SOD remain relatively minor during the simulation interval.

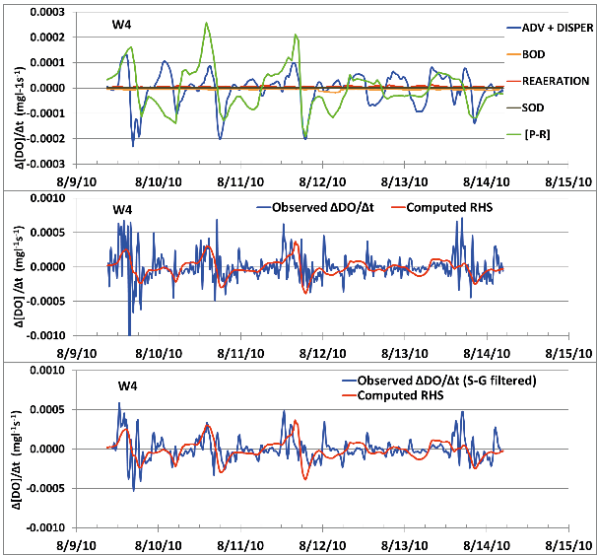

Figure 6: Computed DO dynamic balance at station W4 during intensive field survey. Upper panel: comparison of the calculated fate and transport processes (on right side of Eq. 3). Middle panel: comparison of the calculated time rate of change of observed oxygen concentration with the sum of simulated fate and processes (in upper panel). Bottom panel: same as the middle panel, but with 1-hour running average applied to the raw DO measurement data.

Similar to the P-R term, the model simulates a relatively large advective transport term. However, it does not reproduce very short-period variability (<3 hours) or peaks. An interesting feature at station W4 is the high

degree of 'observed' DO variability (Fig. 6, middle panel). This highly transient response is sometimes apparent even with data smoothing applied (Fig. 6, lower panel). Such short-term (high-frequency) variability also may be associated with complex photosynthesis and respiration processes that are not captured by simplified model formulations (such as the Steele and Arrhenius formulations used here). This effect illustrates a potential limitation of some water quality model formulations, as revealed by high-temporal-resolution DO monitoring data.

The decomposed fate and transport terms were subsequently integrated (using a simple Simpson Rule integration scheme in a spreadsheet format) to simulate a DO time series at station W2 (Fig. 7). This figure provides insight into the effects of the various dynamic processes on the resulting DO concentration.

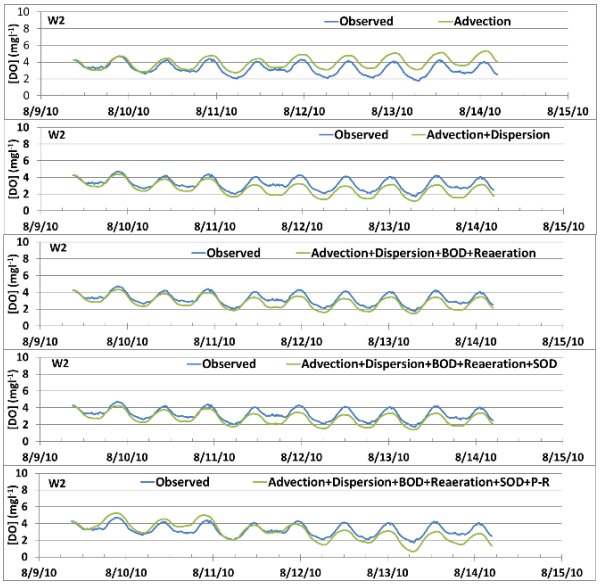

Figure 7: Comparison of observed DO variations at station W2 vs. contributions from various processes.

Fig. 7 (top panel) demonstrates that advective and dispersive transport predominantly explain the observed DO variability at this station. The individual plots in Fig. 7 isolate contributions from other basic processes controlling the dynamics of DO . By incorporating contributions from all terms in the integrations (especially BOD in the latter half), the simplified model can track some observed DO variations (Fig. 7, lowermost panel).

The integrations of the fate and transport terms at the upper estuary station W4 are plotted in Fig. 8. The integration of all terms provides a less accurate fit to the observed DO variability at this station. In this case, the predominance of tidal controls is diminished. Clearly, the model is less accurate when it simulates processes other than tidal displacements of a mean concentration gradient. Also, high frequency variability is noticeable in the monitored DO time series (Fig. 8, lowermost panel) but not in the diagnostic model results.

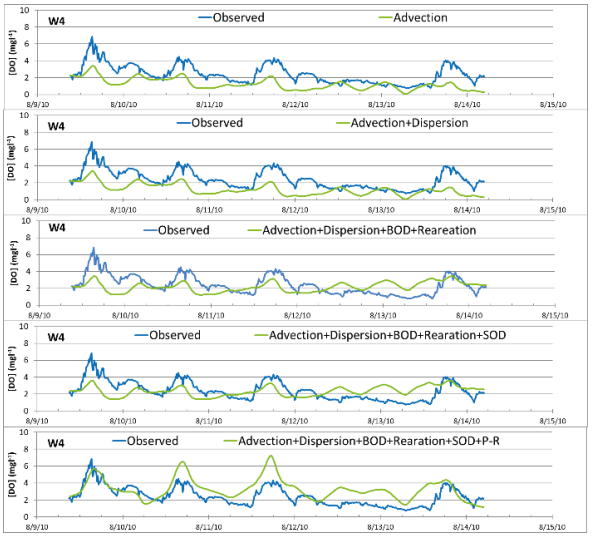

Figure 8: Comparison of observed DO variations at station W4 vs. contributions from various processes.

4 DISCUSSION

Variability on short temporal scales poses difficult challenges to the field of oceanography (McGillicuddy et al., 2017). These high frequency fluctuations can complicate the interpretation of longer-term trends in the mean properties of the physical, biological, and chemical characteristics of the marine environment. However, such fluctuations may be significant in their own right, and may actually contribute to the overall mean properties (e.g., Eq. 8).

The study presented herein illustrates the utility of a simple fate and transport model primarily based on continuous monitoring data for the purpose of synthesizing existing information and quantifying factors influencing short-term DO variability. In this specific case, both continuous

monitoring data and discrete survey data were accessible for a concurrent time frame. Furthermore, the studied waterway is characterized by its narrowness and the dominance of tides and up-estuary sources. This convergence of data availability and simplified environmental conditions offered an opportunity for the preliminary assessment of basic estuarine fate and transport processes. Moreover, it served as an illustration of a scenario in which DO variability may be modeled in an estuarine reach without an immediate necessity for an extensive numerical analysis of the many biogeochemical processes that control DO.

Although not intended to replace more comprehensive hydrodynamic/ water quality models, a 'first-cut' diagnostic model evaluation may offer some advantages, such as simplicity and transparency, which may be absent in some complex numerical models. Moreover, by directly addressing the continuous DO time series data, the simplified model illustrates the potential of such data to identify dominant processes and potential limitations of infrequent sampling. Depending on the variability of dominant controls and other factors, intermittent sampling may fail to capture substantial short-term variability.

The moored arrays yielded high-temporal-resolution DO monitoring data, which introduces additional challenges for model validation. In this case, the continuous (i.e., 15-minute) sampling rate can capture DO, temperature and salinity fluctuations with periods as short as 30+ minutes (based on the well-known, Nyquist sampling theorem). In contrast, the supporting discrete sampling data (e.g., chlorophyll a, CBOD5, NBOD5, TKN, NH3, NO2, TP, OP, etc.), which were collected at three-hour intervals, can only discern fluctuations with periods as short as 6+ hours (i.e., approximately quarter-diurnal). Consequently, the discrete samples were unable to detect shorter-term variability (i.e., < 6 hours). Moreover, the modeled kinetic processes (such as oxygen production and respiration) that depend on such variables, also failed to resolve variations at periods shorter than 6 hours. Thus, it is not surprising that the simplified model does not replicate some of the transients ('spikes') in the 'observed' DO transport, especially at station W4 (Figs. 5-6, middle panels). However, the model otherwise tracked the general temporal trends in the observed data. Therefore, it appears that the lack of comparable resolution of the discrete sampling data did not substantially impede the ability of the model to track diurnal and semi-diurnal (i.e., 12.4-hour-period) variability in the lower reaches of the HRE (Fig. 7, lower panel). In this urbanized, mesotidal estuary -- where tidal displacements and point-source discharges are large – semi-diurnal tidal fluctuations can dominate (e.g., Fig. 6), thereby extending beyond the direct impact area of the discharge.

While the focus of this paper is on tidal transport and short-term variability, it is essential to acknowledge that the simplified model relies on a relatively brief and intensive monitoring period (5 days). Consequently, it does not encompass the simulation of seasonal DO trends. The model also omits the representation of long-term effects of DO sinks (e.g., UBOD decay. Instead, the emphasis is on short-term variability, and the model serves as an adequate tool to evaluate the effects of such sinks over the 5-day study period.

For example, in Fig. 9 (bottom panel), the impact of UBOD removal is illustrated. Figs. 5-6 suggest that while important, UBOD may not constitute the dominant control of DO variability at stations W2 and W4. Fig. 9 further suggests that a hypothetical scenario involving the complete removal of UBOD at station W2 would increase DO levels by about 1 mg/l at station W2 during this particular period. However, it is essential to note that to comprehensively simulate the various seasonal biogeochemical processes associated with UBOD, extended sampling and more intricate modeling efforts would be requisite.

This example underscores the need for an improved diagnostic model designed to more precisely quantify the various sources, sinks and transformation processes over a longer simulation interval (e.g., several weeks). Alternatively, a more detailed diagnostic model may be used to target a short-term event triggered by a large change in loading (e.g., hypoxia following an algal bloom and crash event, or a wastewater treatment plant upset following a catastrophic storm).

In addition to the constraints posed by sampling resolution and duration, it is possible that simple P-R formulations (such as those employed here) may fall short in simulating the exceedingly ephemeral dynamics of algal effects, as evidenced by the continuous monitored DO data. That is, not only are observed peaks of chl-a (Fig. 3) inadequately resolved by 3-hour sampling, but also their transient effects on DO levels may not be resolved using relatively smooth formulations for P-R (unless the model formulation is adapted to accommodate such highly variable algal biomass).

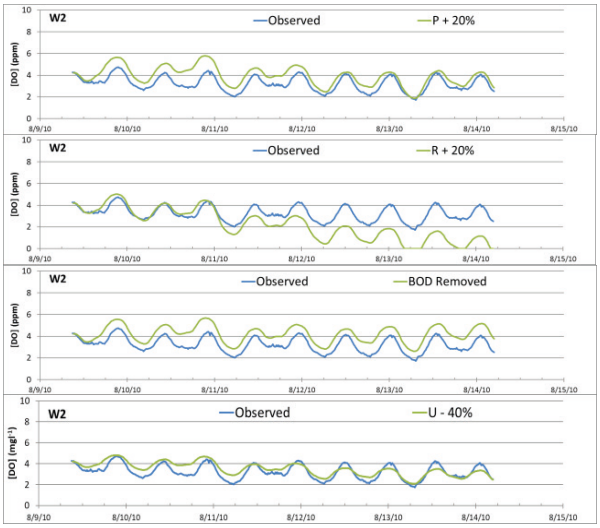

Figure 9: Model sensitivity analysis for simulated DO at station W2: Top panel: base case (from Fig. 7). Second panel from top: effect of 20% increase in photosynthesis. third panel: effect of 20% decrease in respiration. fourth panel: model scenario simulation of complete BOD removal. Bottom panel: effect of 40% decrease in current speed.

Another constraint of the model lies in the semi-empirical nature of the adjustable model parameters. While, in most instances, conventional literature values were selected, some degree of engineering judgment was still required to fine tune the model. Unfortunately, it is difficult to impose restrictions on this selection process so as to yield a unique solution and and a clear-cut alignment with the observed continuous data, even when employing a limited number of rate constants, as demonstrated in Table 2. Fig. 9 (second and third panels) illustrates how sensitive the simplified model is to a variation (+/- 20%) in the most sensitive model coefficients (i.e., the coefficients for the photosynthesis and respiration terms). Such "tuning" may improve the model's performance in comparison to the base case (top panel); however, it lacks a substantive justification. Model uncertainty arising from parameter selection is likely to be compounded if equations for many state variables, each associated with an additional set of rate constants, were to be incorporated (as in common practice).

Hence, numerous factors may contribute to model uncertainty in this case. These include aspects such as data representativeness, data smoothing techniques, the inherent approximations of finite differencing schemes (1^{st}- and 2^{nd}-order accurate), the employment of the Simpson rule integration scheme (2^{nd} order accurate), and the selection of model rate coefficients. For example, over an extended model run, errors in the integration scheme may accumulate and require corrections. This could potentially explain certain disparities between the observed and simulated DO concentrations at the end of the simulations. However, model sensitivity results indicate that other influential factors significantly contribute to these disparities.

From a practical standpoint, the outcomes of this study may provide insights into the potential ramifications of sedimentation and shoaling on DO levels within comparable estuarine environments. Shoaling enhances the effect of bottom friction, dissipates tidal energy, and generally results in reduced current speeds. In such cases, the present model forecasts a corresponding decrease in advective DO transport, and a reduction in the range of DO variability. For example, Fig. 9 (lower panel) displays effects of a 40% decrease in the input current speed, which results in a shallower DO response, with reduced DO tidal variability compared to the base case shown in Figure 7 (bottom panel).

Alternatively, dredging activities and the establishment of dredged material disposal islands have the potential to partially obstruct tidal currents within these narrow estuaries and may increase ('funnel') local current speeds. In such cases, the simplified model suggests that the range of DO variability may increase. Such

conclusions can lend support to ecologically responsible dredged material management initiatives.

The present approach is adaptable for estimating tidal dispersive fluxes as well. To this end, the expression in Eq. 10 was iteratively computed at station W2 and then multiplied by the water density (approximately 1,020 kg/m^3). As a result, a down-estuary tidal dispersive flux of UBOD was determined, exhibiting variations ranging from 0.03 kg/s to 0.79 kg/s. For comparison, the mean 'advective' flux of UBOD at station W2 attributed to river discharge was calculated to be approximately 0.07 kg/s This calculation entails the product of the mean discharge (~ 10.9 m^{3}s^{-1}), the mean UBOD concentration (~ 6 ppm), and mean water density (~ 1,020 kg/m^3). This result suggests that tidal pumping may be a dominant dispersion mechanism in this system. It is important to note that other possible mechanisms may partially contribute to longitudinal dispersion in the HRE, such as vertical/lateral shear or oscillatory shear flow, but these factors have been omitted in the current analysis.

5 CONCLUSIONS

Short-term DO variability is a salient feature of the narrow and tidally influenced HRE. The simplified diagnostic model presented in this study, focusing on the lower HRE, suggests that advective tidal transport stands out as the primary driver of short-term DO variability. Ancillary processes, including UBOD and SOD, appear to exert secondary influences on short-term variability. Furthermore, longitudinal dispersion associated with tidal pumping facilitates the inflow of dissolved oxygen into the lower reaches of the HRE, while exporting UBOD from upstream point sources. The findings of this study suggest that under specific conditions (e.g., for narrow, tidally dominated estuaries with upstream sources), the simple model presented herein proves a valuable tool for amalgamating existing monitoring data, monitoring short-term DO trends, and providing a transparent depiction of the underlying dynamic processes.

The results also indicate that certain smooth model formulations for photosynthesis and respiration may not adequately capture high-frequency variability. To address this issue, high-temporal-resolution data (such as data collected here), and alternative model formulations may be necessary. The simplified spreadsheet format employed in this model may serve as a practical tool to investigate the impacts of alternate water quality model formulations.

ACKNOWLEDGEMENTS
The authors express their gratitude to the Bergen County Utilities Authority for their sponsorship of the field study and a separate numerical model study, conducted in conjunction with NJDEP to address existing impacts in the HRE, thus facilitating long-term facility planning. Additionally, we extend our appreciation to the dedicated staff at ARCADIS, Inc. (especially Mr. Alex Santos) and Malcolm Pirnie, Inc. (especially Mr. Mark Kosakowski) for theirinvaluable contributions to field coordination and the complex monitoring program's design and implementation. We are also grateful to the reviewers and the editor for their helpful comments. Preparation of this manuscript and the decision to submit it for publication were conducted and funded internally by Najarian Associates.

NOTATION
The following symbols are used in this paper:
t = time;
x = along-axis distance (positive landward);
u = vertically averaged, along axis current velocity component (positive landward);
η = water surface elevation
ρ = water density
g = gravitational acceleration
h = average water depth
CD = drag coefficient
[DO] = dissolved oxygen concentration;
$[DO]_s$ = dissolved oxygen saturation concentration
[UBOD] = ultimate carbonaceous BOD
[UNBOD] = ultimate nitrogenous BOD
SOD = sediment oxygen demand
K = Longitudinal (along-channel) dispersion coefficient
I = irradiance
I_s = saturation value of the irradiance
T = water temperature

k_C = CBOD decay coefficient
k_N = ammonia decay coefficient
k_s = Langbein & Durum reaeration rate coefficient ($k_s = 7.6u/h^{1.33}$)
Pm = maximum production rate
k_r = respiration constant
= temperature adjustment factor (typically ~ 1.047)
B = algal biomass
[chl-a] = chlorophyll-a concentration
α = chlorophyll-a to carbon conversion factor
c = constituent concentration

Operators and Superscripts for c and u
< > = tidal average
‘ = tidal fluctuation

REFERENCES

Ahnert, K. and M. Abel, 2007. ‘Numerical differentiation of experimental data: local versus global methods.’ Computer Physics Publications, 177: 764-774., Elsevier, doi:10.1016/j.cpc.2007.03.009.

ARCADIS, 2013. Bergen County Utilities Authority Lower Hackensack River phase II nutrient TMDL study sampling and monitoring report. Unpublished Report to the Bergen County Utilities Authority, Little Ferry, NJ.

Churchill, M., Elmore, H., and R. Buckingham, 1962. The prediction of stream reaeration rates. *Journal of the Sanitary Engineering Division, ASCE*, 88(SA4):1-46.

Chartrand, R. 2011. Numerical Differentiation of Noisy, Nonsmooth Data. International Scholarly Research Network, ISRN Applied Mathematics, Vol. 2011, Article ID 164564, 11 pp. doi:10.5402/2011/164564

DiLorenzo, J., Filadelfo, R., Surak, C., Litwack, H., Gunawardana, V. and T. Najarian, 2004. ‘Tidal variability in the water quality of an urbanized estuary.’ *Estuaries*, 27(5), 851-860.

Dyer, K., 1977. Estuaries A Physical Introduction, 2nd Edition. West Sussex (England): John Wiley & Sons, Ltd.

Fischer, H., List, E., Koh, R., Imberger, J., and N. Brooks, 1979. Mixing in Inland and Coastal Waters. New York: Academic Press.

Foote, M., 1983. The spatial and temporal distribution of suspended algae and nutrients in the upper Hackensack River Estuary. Ph. D. Thesis, Rutgers University, New Brunswick, New Jersey.

Fram, J., Martin, M., and M. Stacey, 2007. Dispersive Fluxes between the Coastal Ocean and a Semi-enclosed Estuarine Basin. *Journal of Physical Oceanography, 37(6): 1,645-1,660.*

Ganju, N., Brush, M., Rashleigh, B., Aretxabaleta, A., del Barrio, P., Grear, J., Harris, L., Lake, S., McCardell, G., O’Donnell, J., Ralston, D., Signell, R., Testa, J., and J. Vaudrey, 2016. ‘Progress and challenges in coupled hydrodynamic-ecological estuarine modeling.’ Estuaries and Coasts, 39, 311-332.

Geyer, W.R., and R. Signell, 1992. ‘A reassessment of the role of tidal dispersion in estuaries and bays.’ *Estuaries 15*(2): 97-108.

Hubertz, E. and L. Cahoon, 1999. Short-term variability of water quality parameters in two shallow estuaries of North Carolina. *Estuaries* 22(3), 814-823.

Ji, Z.-G., 2017, 2007. Hydrodynamics and water quality. Modeling rivers, lakes and estuaries. New Jersey: John Wiley & Sons, Inc.

Jung, H., Richards, J. and A. Fitzgerald, 2021. Temporal and spatial variations of water quality in the Newark Bay Estuary’ Regional Studies in Marine Science, Elsevier, 41 (2021) 101589.

Langbein, W. and W. Durum, 1967. The Aeration Capacity of Streams. U.S. Geological Survey Circular 542. United States Department of the Interior, Washington, DC.

LeBlond, P., 1978. ‘On tidal propagation in shallow rivers.’ *Journal of Geophysical Research, Oceans*, 83(C9), 4717-4721.

Lovato, T., Ciavatta, S., Brigolin, D., Rubino, A. and R. Pastres, 2013. ‘Modelling dissolved oxygen and benthic algae dynamics in a coastal ecosystem by exploiting real-time monitoring data.’ *Estuarine, Coastal and Shelf Science,* 119, 17-30.

Lucas, L., Sereno, D., Burau, J.R., Schraga, T., Lopez, C., Stacey, M., Parchevsky, K. and V. Parchevsky, 2006. Intradaily variability of water quality in a shallow tidal lagoon: Mechanisms and implications. *Estuaries and Coasts*, 29(5), 711-730.

Lucas, L., 2010. Implications of estuarine transport for water quality. In: Contemporary issues in estuarine physics. Valle-Levinson, A. (ed.), Cambridge: Cambridge University Press.

Lung, W. 1993. Water Quality Modeling Volume III Application to Estuaries. New York: CRC Press, Inc.

Marr, W.A., Ladd, C.C., and P.J. Fox, 2014. 'Guidelines for Writing a Case Study Paper.' *Journal of Geotechnical and Geoenvironmental Engineering,* 140(3). DOI: 10.1061/(ASCE)GT.1943-5606.0001076 < https://ascelibrary.org/doi/10.1061/%28ASCE%29GT.1943-5606.0001076> (Aug. 2, 2019).

McGillicuddy, D.J., Budillon, G., and A. Kustka, 2017. Mesoscale and high-frequency variability in the Ross Sea (Antarctica): An introduction to the special issue. *Journal of Marine Systems*, (166), 1-3

Nezlin, N.P., Kamer, K., Hyde, J. and E. Stein, 2009. 'Dissolved oxygen dynamics in a eutrophic estuary, Upper Newport Bay, California.' *Estuarine, Coastal and Shelf Science,* 82: 139-151.

Najarian Associates, 1990. Impact analysis of sewage treatment plant discharges on the water quality of the lower Hackensack River. Unpublished report to the Bergen County Utilities Authority, Little Ferry, NJ.

Najarian Associates, 2015. Lower Hackensack River nutrient TMDL study Data Characterization Report. Report to the Bergen County Utilities Authority, Little Ferry, NJ.

Shen, J., Wang, T., Herman, J., Mason, P., and G.L. Arnold, 2008. 'Hypoxia in a coastal embayment of the Chesapeake Bay: A model diagnostic study of oxygen dynamics.' *Estuaries and Coasts*, 31, 652-663.

Stavitzky, A. and M.J. Golay, 1964. Smoothing and differentiation of data by simplified least squares procedures. *Analytical Chemistry*, 36; 166627-1639.

Steele, J., 1962. Environmental control of photosynthesis in the sea. *Limnology and Oceanography*, 7:137-150.